Journal of Alloys and Compounds 503 (2010) 439–444

Contents lists available at ScienceDirect

Journal of Alloys and Compounds

journal homepage: www.elsevier.com/locate/jallcom

Microwave-induced solid-state decomposition of the $Bi[Fe(CN)_6]\cdot 5H_2O$ precursor: A novel route for the rapid and facile synthesis of pure and single-phase $BiFeO_3$ nanopowder

Saeid Farhadi*, Nazanin Rashidi

Department of Chemistry, Lorestan University, Khoramabad 68135-465, Iran

ARTICLE INFO

Article history:
Received 28 March 2010
Received in revised form 2 May 2010
Accepted 4 May 2010
Available online 11 May 2010

Keywords:
Nanopowder
$BiFeO_3$
Chemical synthesis
Perovskite-type oxide
Multiferroic materials
Microwave heating

ABSTRACT

Pure $BiFeO_3$ nanopowders were synthesized through microwave-induced solid-state decomposition of $Bi[Fe(CN)_6]\cdot 5H_2O$ precursor in the presence of CuO powder as strong microwave absorber within a very short reaction time of 6 min. The product was characterized by a variety of techniques such as TGA–DTA, XRD, FT-IR, Raman spectroscopy, SEM, TEM, EDX, UV–vis spectroscopy and magnetic measurement. The magnetic measurement confirms that the product shows a weak ferromagnetic order at room temperature, which may be ascribed to the size confinement effect. The DTA and DSC results confirm multiferroic nature of the prepared $BiFeO_3$ nanopowder with Neel temperature at 371 °C and Curie temperature at 830 °C. The $BiFeO_3$ prepared by this method could be an appropriate visible-light photocatalytic material due to a strong absorption band in the visible region. In comparison with other reported method, this method is simple, fast and energy efficient and resulted in smaller nanoparticles with an average size about 10 nm.

1. Introduction

Multiferroic materials, which exhibit both ferroelectric and magnetic ordering, have been investigated intensively during the last decade due to their potential applications for novel magnetoelectric devices and for exploring fundamental science in the coupling mechanism between electronic and magnetic order parameters [1–3]. Among all multiferroics, $BiFeO_3$ that exhibits the coexistence of ferroelectric and antiferromagnetic orders above room temperature has received great attention due to its relatively high Neel temperature ($T_N \sim 375$ °C) and Curie temperature ($T_C \sim 830$–850 °C) [4]. Because of this magnetoelectric coupling, $BiFeO_3$ based systems may be used to develop novel applications in the field of radio, television, microwave and satellite communication, bubble memory devices, audio-video and digital recording [5–8]. However, multiferroic properties and potential applications of $BiFeO_3$ were greatly hampered by the leakage current arising from impurities, defects or nonstoichiometry, which is mainly due to the difficulty in preparing pure $BiFeO_3$ phase [9,10].

It is well known that $BiFeO_3$ nanostructures exhibit unique electrical, magnetic, and optical properties due to their low dimensionality and quantum confinement effect which is different from the properties of bulk samples [11]. Furthermore, $BiFeO_3$ nanopowder has shown the prominent visible-light photocatalytic activity that is ascribed to the small band gap and the high surface area of nanosized $BiFeO_3$ [11]. These nanosize-induced properties are expected to widen the potential applications of $BiFeO_3$. Although $BiFeO_3$ powders have been synthesized by solid-state reaction of Bi_2O_3 and Fe_2O_3 at temperature greater than 800 °C with the help of nitric acid leaching out the unavoidable impurities, such as $Bi_2Fe_4O_9$ and $Bi_{25}FeO_{40}$ [12–16] but synthesizing the pure single-phase nanosized $BiFeO_3$ is difficult through this simple traditional route.

In recent years various wet chemical methods have been developed to prepare $BiFeO_3$ nanopowders, such as hydrothermal synthesis [17–20], coprecipitation [21], sonochemical and microemulsion techniques [22], combustion synthesis [23–25], ferrioxalate precursor method [26], sol–gel process [27–31], polymeric precursor method [32,33], mechanochemical synthesis [34], EDTA complexing gel process [35], polyacrylamide gel route [36], molten-salt method [37], and tartaric acid-assisted gel strategy [38]. However, each of these methods has its own advantages and limitations. From a practical viewpoint, the development of simpler, energy efficient and environmentally benign procedures to obtain $BiFeO_3$ nanopowder with a regular morphology and a homogeneous chemical composition under milder conditions is still an active area of research.

* Corresponding author. Tel.: +98 661 2202782; fax: +98 661 6200098.
E-mail address: sfarhad2001@yahoo.com (S. Farhadi).

0925-8388/$ – see front matter © 2010 Elsevier B.V. All rights reserved.
doi:10.1016/j.jallcom.2010.05.029

One of the most promising techniques to overcome the above mentioned problems to be the use of microwave heating. This technique offers several unique advantages and significant merits such as easy workup, rapid volumetric heating, high reaction rate, short reaction time, energy saving and production of inorganic nanopowder with narrow size distribution over other methods [39,40]. Various inorganic nanomaterials have been synthesized using microwave irradiation technique for different applications [41–49]. In this context, we have prepared perovskite-type $LaFeO_3$ and $LaCoO_3$ nanopowders via microwave-assisted decomposition of $La[Fe(CN)_6]\cdot 5H_2O$ and $La[Co(CN)_6]\cdot 5H_2O$ precursors, respectively [50,51].

As a new method, in this paper we report a fast, simple and clean route to prepare $BiFeO_3$ nanopowder in pure phase through microwave-induced solid-state decomposition of $Bi[Fe(CN)_6]\cdot 5H_2O$ as a novel precursor. The product was identified by X-ray diffraction (XRD), Fourier-transformed infrared spectroscopy (FT-IR), Raman spectroscopy, UV–vis spectroscopy, scanning electron microscopy (SEM), transmission electron microscopy (TEM), energy-dispersive X-ray spectroscopy (EDX), thermal analyses (DTA–DSC) and vibrating sample magnetometry (VSM).

2. Experimental

2.1. Preparation of $Bi[Fe(CN)_6]\cdot 5H_2O$ precursor

$Bi[Fe(CN)_6]\cdot 5H_2O$ precursor was synthesized on the basis of reported method for $Ln[Fe(CN)_6]\cdot 5H_2O$ complexes with minor modification as follows [52]. $Bi(NO_3)_3\cdot 5H_2O$ (20 mmol) was dissolved in 20 mL of water in the presence of 3 mol/L HNO_3 and mixed with $K_3[Fe(CN)_6]$ (20 mmol) dissolved in 20 mL of water under continuous stirring. The mixture was stirred at room temperature for 30 min. The resulting brownish precipitate was separated and washed with water, ethanol, and diethyl ether and dried in air.

2.2. Preparation of $BiFeO_3$ nanopowder

To prepare $BiFeO_3$ nanopowder, the $Bi[Fe(CN)_6]\cdot 5H_2O$ precursor powder (1 g) was taken in a small porcelain crucible and was placed in the middle of another larger porcelain crucible filled with CuO powder as a secondary microwave absorber. This assembly was then exposed to microwaves in a microwave cavity (LG–intellowave, 900 W, 2.45 GHz) operated at the power level of 360 W (40%) in air. During microwave irradiation with 300 W output, the CuO powder became fully red hot and its temperature was elevated from room temperature to 620 °C, as measured by quickly inserting of a chromel–alumel thermocouple into the reaction mixture. At the same time, decomposition of the precursor powder was initiated which was completed after an irradiation time of 6 min. The decomposition product was cooled to room temperature and collected for the characterization.

2.3. Characterization

The crystal structure and phase compositions of the obtained product were identified with a Bruker D4 Advance X-ray diffractometer using Cu Kα radiation (λ = 0.15418 nm). Infrared spectra were recorded on a Schimadzu system FT-IR 160 spectrophotometer using KBr pellets. Thermogravimetry (TG) of precursor and differential thermal analysis-differential scanning calorimetry (DTA–DSC) of product were performed in a Netzsch STA 409 PC/PG simultaneous thermal analyzer at a heating rate of 10 °C/min. Raman spectrum measurement was carried out on a Spex 1403 Raman spectrometer. Optical absorption spectrum was recorded on a Shimadzu 1650PC UV–Vis spectrophotometer with the wavelength rang of 300–700 nm at room temperature. The sample for UV–vis studies was well dispersed in distilled water to form a homogeneous suspension by sonicating for 25 min. The powder morphology was observed by a scanning electron microscope (SEM, Philips XL-30) equipped with a link energy-dispersive X-ray (EDX) analyzer. The particle size was determined by a transmission electron microscope (TEM, LEO-906E) at an accelerating voltage of 80 kV. A vibrating sample magnetometer (VSM) was used to measure the magnetic properties of $BiFeO_3$ nanopowder.

3. Results and discussion

In order to use microwave energy at least one of the reactants should be a microwave absorber. In the present study, $BiFeO_3$ nanopowder was prepared through microwave-induced decomposition of $Bi[Fe(CN)_6]\cdot 5H_2O$ precursor in the presence of CuO. In a control experiment, the $Bi[Fe(CN)_6]\cdot 5H_2O$ remained unchanged after 25 min of irradiation without CuO, confirming that this material does not absorb microwaves and needs to a secondary absorber such as CuO. Under this condition, the microwave radiation is mainly absorbed by the CuO powder, so that its temperature went up abruptly from room temperature to 620 °C. The precursor sample is then decomposed by the hot heating medium of CuO at 620 °C and the ultrafine $BiFeO_3$ powder was obtained within several minutes. It seems that the decomposition of $Bi[Fe(CN)_6]\cdot 5H_2O$ was accompanied by the evolution of various gases (such as CO_2, NO_x and water vapor) and this gas evolution resulted in a ultrafine powder. The microwave reaction involved in the formation of $BiFeO_3$ is as follows: $Bi[Fe(CN)_6]\cdot 5H_2O \xrightarrow[\text{solid-state decomposition}]{MW+CuO} BiFeO_3 + 6CO_2 + 6NO_x + 5H_2O$

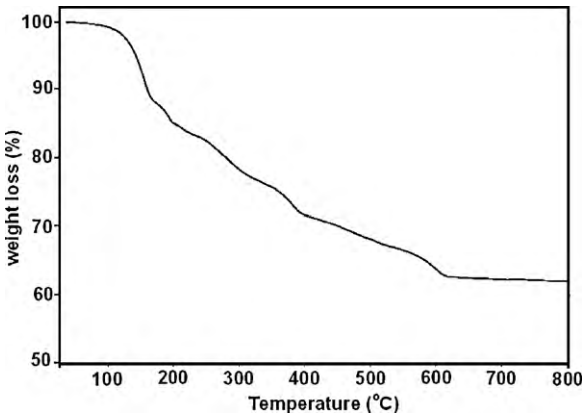

Fig. 1. TGA curve of $Bi[Fe(CN)_6]\cdot 5H_2O$ precursor.

In order to investigate the thermal behavior of the precursor, its thermogravimetric analysis was shown in Fig. 1. From TGA curve, two major distinct weight losses are observed. The first major weight loss occurs at 110–225 °C is attributed to the evaporation of five molecules of crystalline water. The second major weight loss starts at 260 °C and followed by a gradual weight loss until 600 °C is due to the decomposition of the cyanide groups. The weight losses of these two steps to be 17% and 21%, respectively, which are close to the theoretical values. The total weight loss is about 38%, which is close to the theoretical value (38.54%) for the formation of $BiFeO_3$ according with the above chemical equation. Furthermore, this finding confirms the composition of $Bi[Fe(CN)_6]\cdot 5H_2O$ precursor.

Fig. 2 shows the XRD patterns of the $Bi[Fe(CN)_6]\cdot 5H_2O$ precursor complex and its decomposition product. The XRD pattern for the complex (Fig. 2(a)) is similar with those that reported in literature for $La[Fe(CN)_6]\cdot 5H_2O$ (JCPDS File No. 25-1198) and $La[Co(CN)_6]\cdot 5H_2O$ (JCPDS File No. 36-0674), revealing that the structure of $Bi[Fe(CN)_6]\cdot 4H_2O$ is identical with these well known complexes [52]. Fig. 2(b) shows the XRD pattern of the obtained product from the decomposition of $Bi[Fe(CN)_6]\cdot 5H_2O$. From the comparison with Fig. 2(a), it is very clearly evident that all diffraction peaks related to the precursor were disappeared and new peaks were observed. The observed peaks can be readily attributed to the pure rhombohedrally distorted perovskite-type $BiFeO_3$ with lattice parameters of $a = b = 5.576$ Å and $c = 13.867$ Å [space group: *R3c* (No. 161)], which are in good agreement with the reported data (JCPDS, File No. 86-1518). The slight splitting of peak at $2\theta = 32$ confirms rhombohedral symmetry of $BiFeO_3$. The diffraction angle and intensity of the characteristic peaks are well consistent with those of the standard JCPDS card of $BiFeO_3$. No characteristic XRD

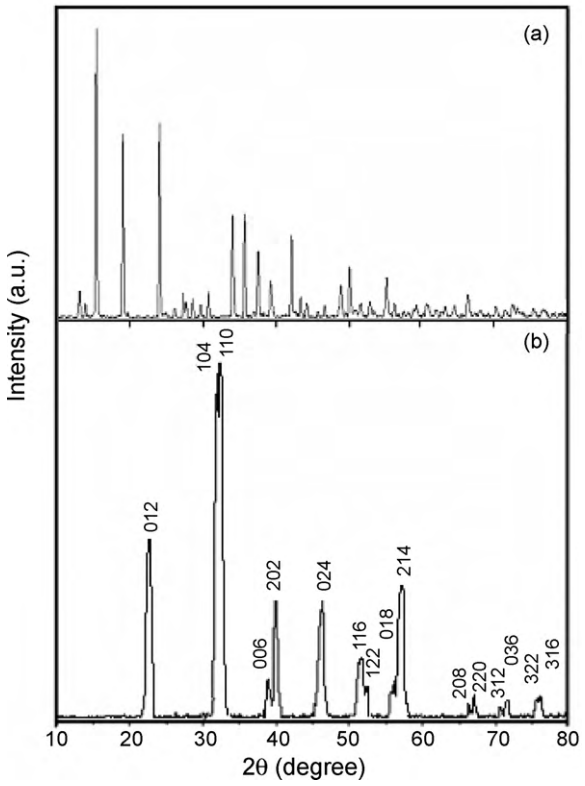

Fig. 2. XRD pattern of (a) $Bi[Fe(CN)_6]\cdot 5H_2O$ precursor and (b) $BiFeO_3$ nanopowder.

peaks of possible impurity phases such as Fe_2O_3, Bi_2O_3, $Bi_2Fe_4O_9$, $Bi_{25}FeO_{40}$ and unreacted precursor were observed, indicating the preparation of pure single-phase $BiFeO_3$ by this method. It can be seen from Fig. 2(b) that the diffraction peaks are markedly broadened due to the small size effect of the particles. The average crystallite size obtained from the Debye–Scherrer formula is ~10 nm [53].

The FT-IR spectra of $Bi[Fe(CN)_6]\cdot 5H_2O$ precursor and its product are shown in Fig. 3. In the FT-IR spectrum of precursor (Fig. 3(a)), the sharp band at about 2140 cm^{-1} is attributed to the stretching of C≡N groups while the bands at 400–600 cm^{-1} are related to the vibrations of Fe–CN bonds [54]. Also, the broad band at 3000–3600 cm^{-1} and a band at about 1625 cm^{-1} are corresponded to the stretching and bending vibrations of the lattice water molecules, respectively [54]. As can be seen in Fig. 3(b), all of these bands were eliminated after the microwave-assisted decomposition of this precursor. In the FT-IR spectrum of the product (Fig. 3(b)), two strong bands around 560 and 440 cm^{-1} are related to the Fe–O stretching and bending vibrations, respectively, being characteristics of the octahedral FeO_6 groups in the perovskite compounds [55].

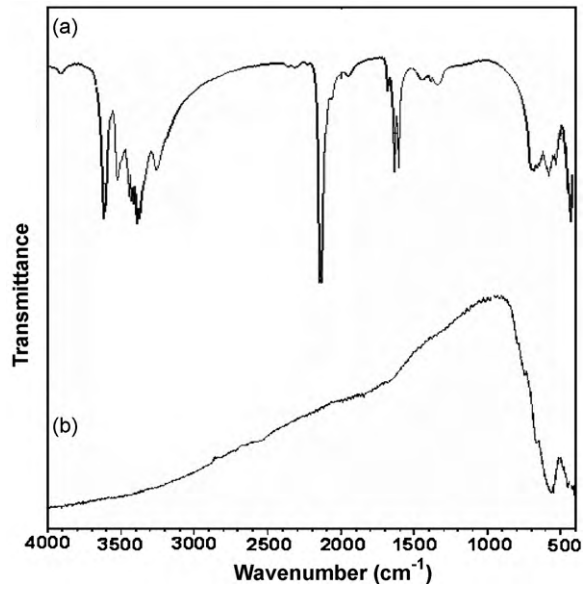

Fig. 3. FT-IR spectra of (a) $Bi[Fe(CN)_6]\cdot 5H_2O$ precursor and (b) $BiFeO_3$ nanopowder.

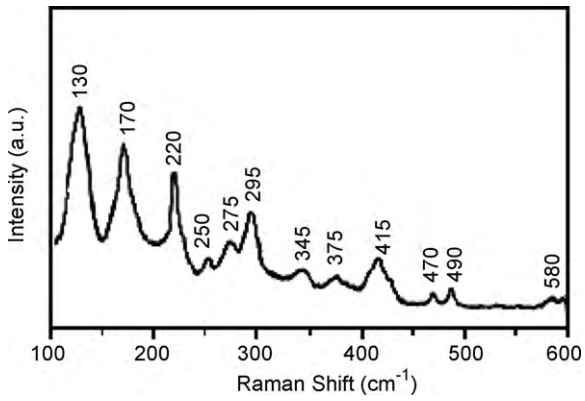

Fig. 4. Raman spectrum of $BiFeO_3$ nanopowder.

Fig. 4 exhibits Raman spectrum of the obtained $BiFeO_3$ nanopowder in the range of 100–600 cm^{-1}. There are characteristic lines at around 130, 170, 220, 250, 275, 295, 345, 375, 415, 470, 490 and 580 cm^{-1} in the Raman spectrum of product, which are similar to those of $BiFeO_3$ reported in the literature [32,34]. On the other hand, the widening of these lines suggests that the size of particles is very small [56].

The morphologies of $Bi[Fe(CN)_6]\cdot 5H_2O$ and its decomposition product were investigated by SEM as shown in Fig. 5. The SEM micrograph of $Bi[Fe(CN)_6]\cdot 5H_2O$ powder in Fig. 5(a) shows that it was made of large polyhedron crystals with sharp edges up to 3 μm in size. The SEM micrograph of the product powder in Fig. 5(b) clearly shows that the shape and morphology of the $BiFeO_3$ is quite different with that of its precursor complex. As can be seen, the large polyhedron grains of precursor were completely disrupted and extremely fine particles which loosely aggregated were appeared. Because of the extremely small dimensions and high surface energy of the obtained $BiFeO_3$ particles, it is easy for them to aggregate as seen in Fig. 5(b).

The EDX microanalysis was performed in situ by selecting single particles randomly in the SEM image (Fig. 6). The atomic proportions of Bi and Fe in the powder determined by EDX are 49.72% and 50.28%, respectively. The ratio of Bi and Fe is almost 1:1, further demonstrating that pure $BiFeO_3$ phase was synthesized successfully and Bi-rich phases such as $Bi_2Fe_4O_9$, $Bi_{25}FeO_{40}$ and $Bi_{36}Fe_{24}O_{57}$ were not formed. The EDX spectroscopy cannot determine the atomic proportion of light element such as oxygen.

TEM image of the $BiFeO_3$ powder is presented in Fig. 7. The TEM image reveals that the powder is composed of aggregated semi-spherical nanoparticles with an average size about 10 nm. This is consistent with the average size obtained from the XRD pattern.

UV–vis spectroscopy has been employed to characterize the optical properties of the $BiFeO_3$ nanopowder. Fig. 8 represents the optical absorption spectrum of the $BiFeO_3$ nanopowder with a relatively strong absorption band in the visible region, indicat-

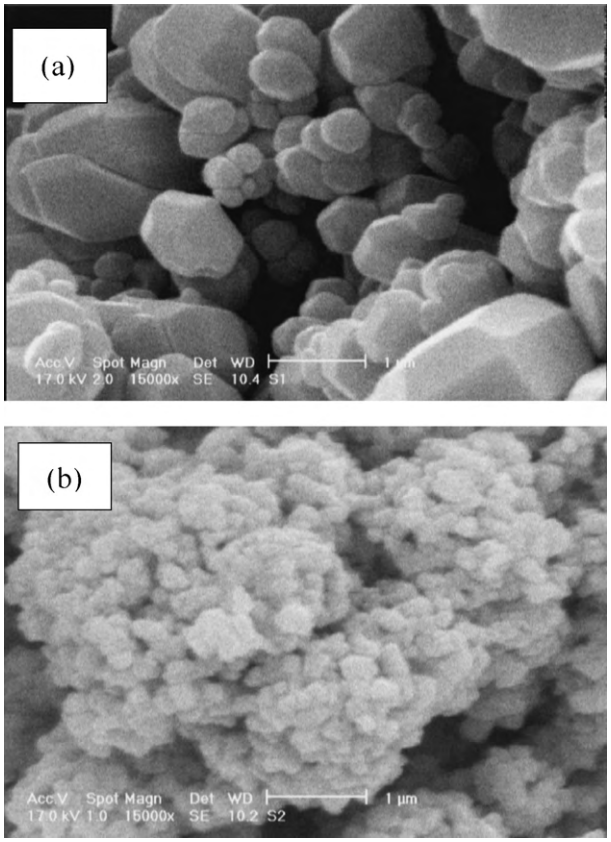

Fig. 5. SEM micrographs of (a) $Bi[Fe(CN)_6]\cdot 5H_2O$ precursor and (b) $BiFeO_3$ nanopowder (scale bars = 1 μm).

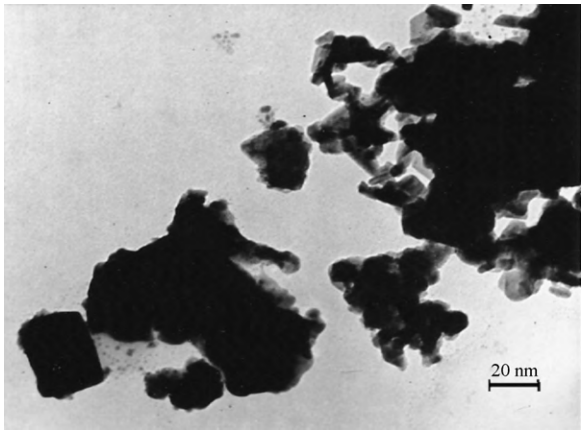

Fig. 7. TEM image of $BiFeO_3$ nanopowder.

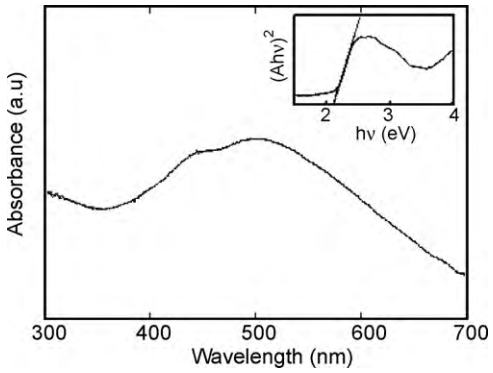

Fig. 8. Optical absorption spectrum of $BiFeO_3$ nanopowder.

ing that the $BiFeO_3$ nanopowder prepared by this method could be a kind of visible-light photocatalytic material. This absorption band is attributed to the electronic transition from the valence band to conduction band ($O^{2-}{}_{2p} \rightarrow Fe^{3+}{}_{3d}$) in $BiFeO_3$ lattice. The optical band gap, E_g, can be determined by the equation $(Ah\nu)^2 = B(h\nu - E_g)$, where $h\nu$ is the photo energy in eV, A is the absorption coefficient, and B is a constant relative to the material [57]. The inset of Fig. 8 indicates the $(Ah\nu)^2$–$h\nu$ curve for the sample in which energy band gap determined by extrapolating the linear portion of this curve to zero. The E_g for the $BiFeO_3$ nanopowder is about 2.2 eV, which is consistent with previous reports [11,20].

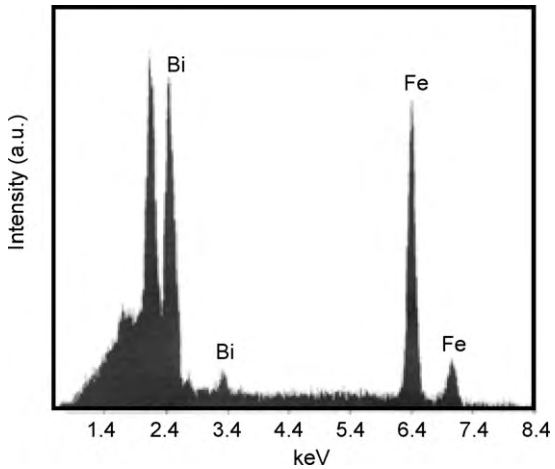

Fig. 6. EDX spectrum of $BiFeO_3$ nanopowder.

Fig. 9 shows the variation of magnetization of the $BiFeO_3$ nanopowder with an applied magnetic field. A typical magnetic hysteresis loop was observed, indicating that the $BiFeO_3$ nanopowder shows a weak ferromagnetic order at room temperature, which is quite different from the linear magnetization–magnetic field relationship in the bulk [19]. The similar ferromagnetic phenomenon was also observed for other $BiFeO_3$ nanostructures [10,11,17,31,38]. The origin of the weak ferromagnetic property

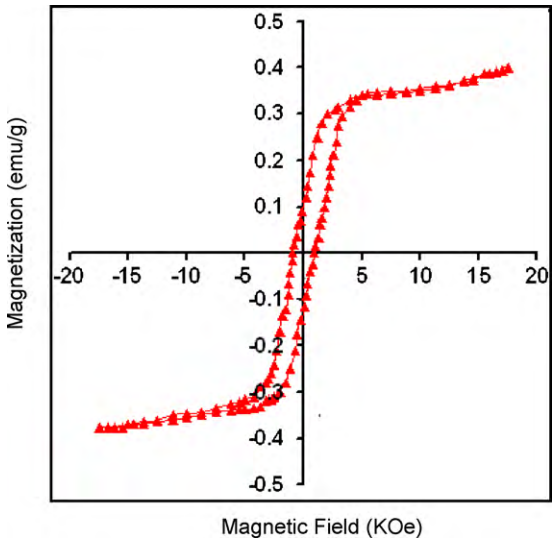

Fig. 9. Magnetization–field hysteresis loop of $BiFeO_3$ nanopowder at room temperature.

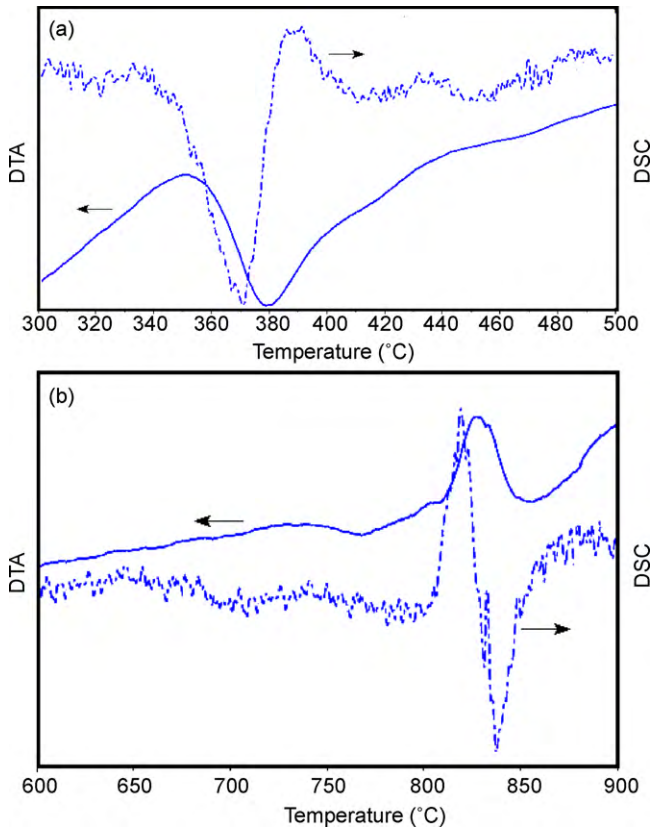

Fig. 10. DTA–DSC curve of $BiFeO_3$ nanopowder in two temperature intervals: (a) 300–400 °C and (b) 600–900 °C.

may be attributed to the size confinement effect of the $BiFeO_3$ nanopowder [11,38].

DTA–DSC thermal analysis was performed on the $BiFeO_3$ nanopowder to determine its Neel and Curie temperatures. The result of DTA–DSC measurements in two temperature intervals of 300–500 and 600–900 °C are shown in Fig. 10. The peak at about 371 °C in Fig. 10(a) is related to a magnetic phase transition (Neel temperature, T_N) and the distinct peak at around 830 °C in Fig. 10(b) is attributed to the ferroelectric-to-paraelectric phase transition (Curie temperature, T_C) of the $BiFeO_3$ nanopowder. The Neel and Curie temperatures of our sample are consistent with previous reports [17,33,35,36]. The DTA and DSC results confirm the multiferroic properties of our $BiFeO_3$ nanopowder, because it presents the almost same Neel temperature (T_N) and ferroelectric Curie temperature (T_C) as those of bulk $BiFeO_3$. However, there is no agreement on the values of the Neel and Curie points for $BiFeO_3$ reported by various research groups [17,24,38]. It seems that these temperatures could vary slightly depending on the processing conditions.

4. Conclusions

In conclusion, in this paper pure $BiFeO_3$ nanopowders with average particle size of 10 nm have been successfully synthesized through the decomposition of the $Bi[Fe(CN)_6]\cdot 5H_2O$ precursor under microwave heating in the presence of CuO as the secondary heater at 620 °C. The preparation of single-phase $BiFeO_3$ with smaller nanoparticles and shorter reaction time are the significant advantages of this simple and novel method as compared with other reported methods. $BiFeO_3$ nanopowder prepared by this method showed a weak ferromagnetic order at room temperature and could be a promising visible-light photocatalytic material due to a strong absorption band in the visible region. Study on the photocatalytic applications of $BiFeO_3$ nanopowder prepared in this work and also the thermal decomposition of the $Bi[Fe(CN)_6]\cdot 5H_2O$ precursor under conventional heating at various temperatures are now in progress in our laboratory.

Acknowledgement

The authors are grateful for the financial support of the Lorestan University Research Council.

References

[1] N. Hur, S. Park, P.A. Sharma, J.S. Ahn, S. Guha, S.W. Cheong, Nature 429 (2004) 392–395.
[2] N.A. Spaldin, M. Fiebig, Science 309 (2005) 391–392.
[3] G.A. Smolenskii, I. Chupis, Sov. Phys. Usp. 25 (1982) 475–493.
[4] S.V. Kalinin, M.R. Suchomel, P.K. Davies, D.A. Bonnel, J. Am. Ceram. Soc. 85 (12) (2002) 3011–3017.
[5] J.D. Bucci, B.K. Robertson, W.J. James, J. Appl. Crystallogr. 5 (1972) 187–191.
[6] F. Kubel, H. Schmid, Acta Crystallogr. 46 (1990) 698–702.
[7] V.R. Palkar, R. Pinto, Pramana, J. Phys. 58 (2002) 1003–1008.
[8] Y.P. Wang, L. Zohu, M.F. Zhang, X.Y. Chen, J.-M. Liu, Z.G. Liu, Appl. Phys. Lett. 84 (2004) 1731–1733.
[9] R. Mazumder, S. Ghosh, P. Mondal, D. Bhattacharya, S. Dasgupta, N. Das, J. Appl. Phys. 100 (2006) 33908–339012.
[10] T.J. Park, G.C. Papaefthymiou, A.J. Viescas, A.R. Moodenbaugh, S.S. Wong, Nano Lett. 7 (2007) 766–772.
[11] F. Gao, X. Chen, K. Yin, S. Dong, Z. Ren, F. Yuan, T. Yu, Z. Zou, J.-M. Liu, Adv. Mater. 19 (2007) 2889–2892.
[12] G.D. Achenbach, W.J. James, R. Gerson, J. Am. Ceram. Soc. 8 (1967) 437–1437.
[13] C. Michel, J.M. Moreau, G.D. Achenbach, R. Gerson, W.J. James, Solid State Commun. 7 (1969) 701–704.
[14] M.M. Kumar, V.R. Palkar, K. Srinivas, S.V. Suryanarayana, Appl. Phys. Lett. 76 (2000) 2764–2766.
[15] J. Li, Y. Duan, H. He, D. Song, J. Alloys Compd. 315 (2001) 259–264.
[16] R.N.P. Choudhary, D.K. Pradhan, G.E. Bonilla, R.S. Katiyar, J. Alloys Compd. 437 (2007) 220–224.
[17] C. Chen, J.R. Cheng, S.W. Yu, L.J. Che, Z.Y. Meng, J. Cryst. Growth 291 (2006) 135–139.
[18] S. Basu, M. Pal, D. Chakravorty, J. Mag. Mag. Mater. 320 (2008) 3361–3365.
[19] Y. Wang, G. Xu, Z. Ren, X. Wei, W. Weng, P. Du, G. Shen, G. Han, J. Am. Ceram. Soc. 90 (2007) 2615–2617.
[20] C.M. Cho, J.H. Noh, I.-S. Cho, J.-S. An, K.S. Hong, J. Am. Ceram. Soc. 91 (2008) 3753–3755.
[21] S. Shetty, V.R. Palkar, R. Pinto, Pramana, J. Phys. 58 (2002) 1027–1030.
[22] N. Das, R. Majumdar, A. Sen, H.S. Maiti, Mater. Lett. 61 (2007) 2100–2104.
[23] V. Fruth, D. Berger, C. Matei, A. Ianculescu, M. Popa, E. Tenea, M. Zaharescu, J. Phys. IV 128 (2005) 7–11.
[24] V. Fruth, L. Mitoseriu, D. Berger, A. Ianculescu, C. Matei, S. Preda, M. Zaharescu, Prog. Solid State Chem. 35 (2007) 193–202.
[25] S. Farhadi, M. Zaidi, J. Mol. Catal. A: Chem. 299 (2009) 18–25.
[26] S. Ghosh, S. Dasgupta, A. Sen, H.S. Maiti, Mater. Res. Bull. 40 (2005) 2073–2079.
[27] S. Ghosh, S. Dasgupta, A. Sen, H.S. Maiti, J. Am. Ceram. Soc. 88 (2005) 1349–1352.
[28] M. Kumar, K.I. Yadav, G.D. Varma, Mater. Lett. 62 (2008) 1159–1161.
[29] J.-H. Xu, H. Ke, D.-C. Jia, W. Wang, Y. Zhou, J. Alloys Compd. 472 (2009) 473–477.
[30] J.K. Kim, S.S. Kim, W.-J. Kim, Mater. Lett. 59 (2005) 4006–4009.
[31] J. Wei, D. Xue, Y. Xu, Scr. Mater. 58 (2008) 45–48.
[32] M. Popa, D. Crespo, J.M. Calderon-Moreno, J. Am. Ceram. Soc. 90 (2007) 2723–2727.
[33] S.M. Selbach, M.-A. Einarsrud, T. Tybell, T. Grande, J. Am. Ceram. Soc. 90 (2007) 3430–3434.
[34] I. Szafraniak, M. Polomska, B. Hilczer, A. Pietraszko, L. Kepinski, J. Eur. Ceram. Soc. 27 (2007) 4399–4402.
[35] J. Wei, D. Xue, Mater. Res. Bull. 43 (2008) 3368–3373.
[36] T. Xian, H. Yang, X. Shen, J.L. Jiang, Z.Q. Wei, W.J. Feng, J. Alloys Compd. 480 (2009) 889–892.
[37] X. He, L. Gao, Ceram. Int. 35 (2009) 975–978.
[38] X. Wang, Y. Zhang, Z. Wu, Mater. Lett. 64 (2010) 486–488.
[39] D.M.P. Mingos, D.R. Baghurt, Chem. Soc. Rev. 20 (1991) 1–47, and references cited therein.
[40] K.J. Rao, B. Vaidhyanathan, M. Ganguli, P.A. Ramakrishnan, Chem. Mater. 11 (1999) 882–895.
[41] M. Panneerselvam, K.J. Rao, J. Mater. Chem. 13 (2003) 596–601.
[42] M. Nakayama, K. Watanabe, H. Ikuta, Y. Uchiharu, M. Wakihara, Solid State Ionics 164 (2004) 35–42.
[43] I. Ganesh, B. Srinivas, R. Johnson, B.P. Saha, Y.R. Mahajan, J. Eur. Ceram. Soc. 24 (2004) 201–207.
[44] P. Elomalai, H.N. Vasan, N. Munichandraiah, J. Power Sources 125 (2004) 77–84.
[45] H.Y. Xu, H. Wang, Y.Q. Meng, H. Yan, Solid State Commun. 130 (2004) 465–468.
[46] J. Guo, C. Dong, L. Yang, G. Fu, J. Solid State Chem. 178 (2005) 58–63.
[47] C. Mastrovito, J.W. Lekse, J.A. Aitken, J. Solid State Chem. 180 (2007) 3262–3264.

[48] N. Takahashi, Mater. Lett. 62 (2008) 1652–1654.
[49] X. Song, L. Gao, J. Am. Ceram. Soc. 91 (2008) 3465–3468.
[50] S. Farhadi, M. Momeni, M. Taherimehr, J. Alloys Compd. 471 (2009) L5–L8.
[51] S. Farhadi, S. Sepahvand, J. Alloys Compd. 489 (2010) 586–591.
[52] F. Hulliger, M. Landolt, H. Vetsch, J. Solid State Chem. 18 (1976) 283–291.
[53] H.P. Klug, L.E. Alexander, X-Ray Diffraction Procedures, 2nd ed., Wiley, New York, 1964.
[54] K. Nakamoto, Infrared and Raman Spectra of Inorganic and Coordination Compounds, Part B: Applications in Coordination, Organometallic, and Bioinorganic Chemistry, 6th ed., Wiley, New York, 2009, pp. 110–120.
[55] G.V.S. Rao, C.N.R. Rao, J.R. Ferraro, Appl. Spectrosc. 24 (1970) 436–445.
[56] M.J. Pelletier, Analytical Applications of Raman Spectroscopy, Blackwell Science, Oxford, 1999.
[57] J. Pankove, Optical Processes in Semiconductors, Prentice-Hall, Englewood Cliffs, NJ, 1971.